inter.noise 2014
MELBOURNE AUSTRALIA
16-19 NOVEMBER

Planar laser induced fluorescence imaging of bubble formation

Marcus FEDRIZZI[1]; Julio SORIA[1,2]

[1] Laboratory for Turbulence Research in Aerospace and Combustion,
Department of Mechanical and Aerospace Engineering, Monash University, Clayton, Victoria 3800, Australia
[2] Department of Aeronautical Engineering, King Abdulaziz University, Jeddah, Kingdom of Saudi Arabia

ABSTRACT

A slowly forming underwater gas bubble will grow, form a neck and detach when the neck collapses, emitting a pulse of sound. During the late stage of the neck collapse the acoustic pulse displays a rarefaction and the acoustic compression begins shortly after detachment. This compression appears to coincide with the formation of an internal jet inside the bubble and an understanding of the behaviour of the bubble internal jet is sought in order to understand the origin of the acoustic emission. In this study time resolved high speed imaging of the bubble detachment process has been undertaken using planar laser induced fluorescence (PLIF) illumination. From these images the internal jet development and evolution are investigated as well as the effect of the jet on the instantaneous bubble volume. The link between the internal jet and the surface waves on the bubble is also investigated for insight on their contribution to bubble sound emission.

Keywords: Bubble, Sound, Generation I-INCE Classification of Subjects Number(s): 21, 22.7

1. INTRODUCTION

The slow release of gas from an underwater orifice of radius a generates bubbles which grow and form a neck while still attached to the orifice. As the bubble volume, V increases and the buoyancy force balances the surface tension fixing the bubble to the orifice, the bubble detaches (1). If the gas flow rate into the bubble, Q is below a critical value, Q_{cr}, the bubble detachment volume should be independent of the flow rate and given by (1),

$$Q_{\mathrm{cr}} = \pi \left(\frac{16}{3g^2}\right)^{\frac{1}{6}} \left(\frac{\sigma a}{\rho}\right)^{\frac{5}{6}}, \tag{1}$$

where ρ is the water density, g the gravitational acceleration and σ the surface tension of the gas-liquid interface. The value of V at detachment for $Q < Q_{\mathrm{cr}}$ is expected to be the Fritz volume (1),

$$V_F = \frac{2\pi\sigma a}{\rho g}. \tag{2}$$

As the bubble approaches detachment the neck rapidly collapses, as can be seen in Figure 1, approaching an apparent physical singularity, and when the gas forms a complete closed surface the bubble is said to have pinched off and it will emit a pulse of sound in the process. Some studies have investigated the conditions leading up to the neck collapse (2, 3) and for an air bubble in water it appears that the detachment occurs at lengths smaller than 10 µm (2). While initially the neck collapse is driven by surface tension, it becomes dominated by liquid inertia forcing the gas inwards in the later stages (4). A consequence of the small detachment length-scale is that the bubble surface at the detachment point has a large curvature, resulting in a relatively large pressure difference on either side of the surface. This pressure difference forces the two sides of the now detached gas-liquid interface in opposite directions, one upwards into the bubble and the other downwards towards the orifice.

The retraction of the now separate gas surfaces occurs very rapidly and as a result a small jet of water is entrained into the bubble, as well as into the downwards moving surface. This jet has been observed in large bubbles (5, 6) and large, easy to observe jets can be created in smaller bubbles with high gas flow rates. The internal jets in small bubbles formed under low gas flow rate conditions, are much smaller and more difficult

[1] marcus.k.fedrizzi@monash.edu

to see. The internal jet has been proposed as the driving mechanism of the sound generation of the bubble (7). Czerski and Deane (8) show that the acoustic signal of a bubble detaching begins with a rarefaction during the final stages of the neck collapsing, followed by a compression after detachment and apparently coinciding with the appearance of the internal jet however the authors of that study did not look at the development and evolution of the internal jet in detail.

The acoustic pulse of the bubble is an exponentially decaying sinusoidal signal with a frequency, f which can be predicted using the Minnaert equation (9),

$$f = \frac{1}{2\pi r}\sqrt{\frac{3kp}{\rho}}. \tag{3}$$

This frequency assumes the bubble is a spherical harmonic oscillator of radius r, k is the specific heat ratio of the gas, and p is the liquid static pressure in the region of the bubble. Even though the bubble at formation is non-spherical, Equation 3 provides valid predictions of the acoustic frequency of non-spherical bubbles by considering their volume and finding the equivalent spherical radius. This is due to the wavelength of the sound being much larger than the bubble.

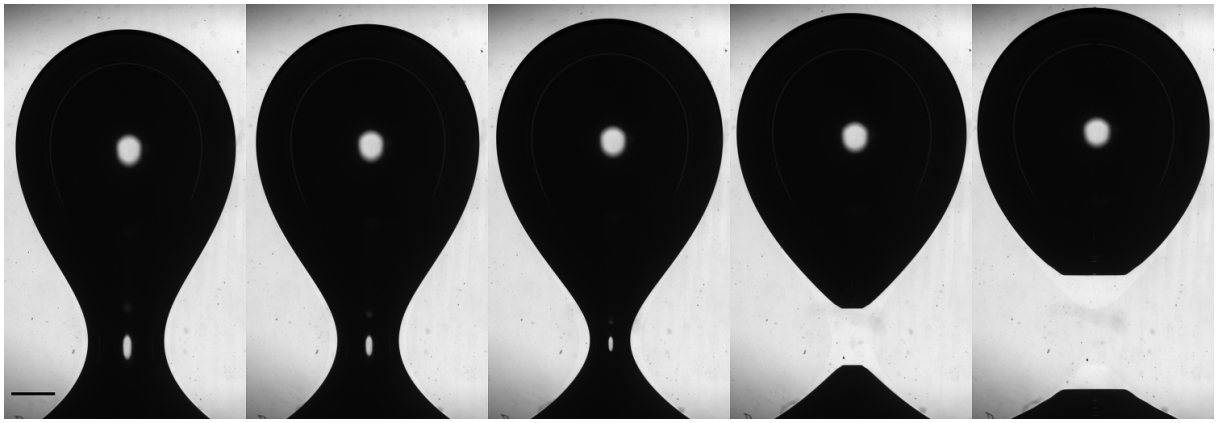

Figure 1 – High speed shadowgraphy images of a bubble detaching from a 2.5 mm radius orifice. Images are 200 µs apart and referred to as A-E from left to right in the text. The black line in the lower left corner indicates 1 mm.

2. EXPERIMENT METHOD

In this study experiments were undertaken to visualise the bubble formation and detachment, specifically looking at the bubble internal jet. The experiments were conducted in an octagonal water tank with 130 mm between adjacent sides with a water depth of 150 mm. A syringe pump was used to generate a small flow rate of air, Q =9.02 mm^3 s^{-1} through an orifice of radius $a = 2.5$ mm. The Weber number, which is a ratio of inertial forces to surface tension forces is defined as,

$$\mathrm{We} = \frac{\rho Q^2}{\sigma a^3}, \tag{4}$$

and Bond number, the ratio of body forces to surface tension, as,

$$\mathrm{Bo} = \frac{\rho g a^2}{\sigma}. \tag{5}$$

Bubbles in the current experiment had Bo = 0.85 and We = 7.2×10^{-5}, under the assumption of a surface tension of 0.072 N m^{-1}. Bubbles were produced at an average rate of one bubble every 9.1 s, with a standard deviation of 0.58 s, from an orifice on a raised stainless steel platform in the center of the tank. A piece of foam used to create a pressure drop before the orifice so that the gas flow rate was constant.

Bubbles were imaged using a PCO Dimax high speed camera at framerates up to 10 kHz and maximum CCD array size of 2016 $\times$ 2016 pixels, with two different magnifications of 2 and 3.8, corresponding to 5.5 µm and 2.9 µm per pixel respectively. In order to achieve high magnification a 200 mm lens was used with a separation of up to 300 mm between the camera and lens.

Shadowgraphy experiments used a high power CBT-120 LED as a backlight with a driver circuit described in (10) and maximum light output at a wavelength of 620 nm. This LED was driven at up to 10 kHz with 2 µs pulses. Laser illumination was from a high speed 527 nm Nd:YLF Quantronix Darwin Duo laser capable of being operated at up to 10 kHz, however due to reduced power at high frequencies this was limited to 5 kHz. The laser beam was formed into a laser sheet, less than 1 mm thick with its waist at the bubble exit.

The timing of laser, LED and camera was controlled with a Stanford Research Systems DG645 delay generator. A photodiode was used to measure the light output from the laser and LED in order to compensate for any delays and synchronise their peak intensity. The small time of the detachment compared to the growth time of the bubble warranted the use of a laser as a trigger to the camera. The laser was set up at a specific height so that as the bubble approached its detachment it would block the laser beam. A photodiode detector was connected to a Beaglebone Black single board computer and was used to trigger the camera to acquire images for a fixed period of time after detecting a falling edge signal.

A small quantity of Kiton Red was added to the water, this is a dye which would fluoresce at about 620 nm under illumination from the green laser light. A Hoya 25A filter was used to block the green 527 nm laser light from reaching the camera while allowing the LED light and light from the fluorescence to pass through. A schematic of the experiment is shown in Figure 2a.

The internal jet which forms inside the bubble immediately after detachment was difficult to image using a shadowgraphy technique of placing the bubbles between a backlight and camera. This difficulty has been noted elsewhere (8), and is because of the curvature of the bubble surface and the change in refractive index at the gas-liquid interface. For light traveling in liquid of refractive index n_l passing through the interface with a gas of refractive index n_g, then the light rays will refract according to Snell's law,

$$\sin\theta_r = \frac{n_l}{n_g}\sin\theta_i, \tag{6}$$

and incidence and refracted angles, θ_i and θ_r, are measured from the surface normal. Because $n_l > n_g$, the light entering the bubble is refracted away from the surface normal, and refracted towards the normal upon exiting the bubble. These refractions result in the light diverging both on entering and exiting the bubble and so only a small amount of light passing through the bubble reaches the camera compared to the large amount of light from the backlight that does not go through the bubble. A 2D simulation of this refraction causing the light to diverge is shown in Figure 2b for an external bubble contour excluding the internal jet. The consequence of refraction through the bubble can be observed in Figure 1 where the light passing through the bubble can be seen in a small circle towards the centre, and also through the neck in frames A-C, where the outward facing surface normal vector points in the camera direction with only a small deviation. In addition to the refraction of light, a ring was observed in the frames of Figure 1 around the upper region of the bubble which is the border of where light is refracted inside the bubble to where light is totally internally reflected in the water. This limits where the camera can see inside the bubble and limits the imaging of the base of the internal jet for this camera configuration.

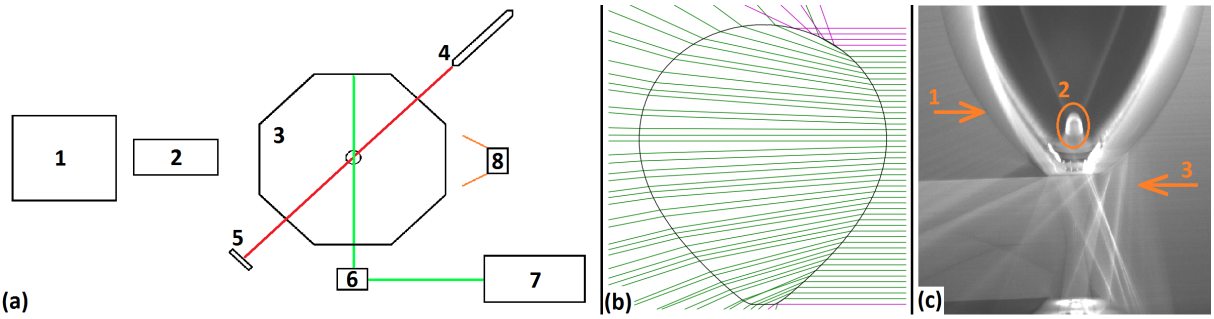

Figure 2 – (a) - Experiment schematic. Numbers indicate: 1 - Camera; 2 - High magnification lens configuration and optical filter; 3 - Octagonal water tank; 4 & 5 - Laser and photodiode detector for bubble trigger; 6 - Optics for high power laser beam focusing and sheet forming; 7 - High speed, high power laser; 8 - High power LED backlight. (b) - Simulated light rays incident on a gas bubble surface showing refracted rays (green) and totally internally reflected rays (magenta). (c) - Example of PLIF imaging of a bubble that has detached with labels indicating: 1 - True bubble edge; 2 - Internal jet; 3 - Reflected light rays indicating surface waves. Note that light is traveling from right to left in b and c.

In order to visualise the internal jet of the bubble a different technique was considered. Planar laser induced fluorescence (PLIF) is a technique which has previously been used on small round bubbles in two phase flows

with a high gas content (11) and in combination with shadowgraphy on larger bubbles in slug flow (12). PLIF imaging of bubbles involves passing a plane of laser light through a bubble in a liquid seeded with fluorescent dye. The camera is placed normal to the plane with an optical filter to remove strong reflections of the laser light off the bubble surface and record only the light from the fluorescence. In the case of imaging the internal jet of a bubble, the jet, containing the liquid will fluoresce, while the gas in the bubble will not. When imaging bubbles using PLIF, see Figure 2c for an example, the true edge of the bubble is not immediately obvious as a result of the light from the fluorescent dye on either side of the bubble being reflected into the camera by the bubble. One technique to overcome this was to combine shadowgraphy and PLIF which enables both the edge of the bubble and internal jet to be imaged. The edge of the internal jet is well defined compared to the bubble edge due to the liquid jet being surrounded by gas which is both not illuminated and will not totally internally reflect any light off the jet into the camera due to light passing to a higher refractive index medium. Imaging the jet through a bubble however is like imaging it through a curved lens and so the jet appears to be taller and thinner than it actually is.

3. RESULTS AND DISCUSSION

From the first image after detachment in Figure 1, the bubble volume V was calculated from the two-dimensional area of the bubble using an edge detection code under the assumption of axisymmetry and revolving this area, A by an angle of π. The edge detection scanned through each row of pixels and extracted the first and last point corresponding to the bubble to subpixel accuracy by finding the local extrema of the derivative. The bubble volume was, $V = 81.1\,\mathrm{mm}^3$ and hence an equivalent radius, r of the bubble if it was spherical $V = \pi A = 4\pi r^3/3$ was $r = 2.68\,\mathrm{mm}$. This result for volume agrees with the volume obtained from the flow rate into the bubble $9.02\,\mathrm{mm}^3\,\mathrm{s}^{-1}$ and production time of 9.1 ± 0.58 s for most bubbles gives a volume of $82 \pm 5.2\,\mathrm{mm}^3$. The flow rate in this experiment is 0.03% of the critical flow rate given by Equation 1. Taking the surface tension of the water as $0.072\,\mathrm{N\,m}^{-1}$, $V_F = 115\,\mathrm{mm}^3$ from Equation 2. Previous studies for these low flow rates found the bubble volume can be expected to be about $0.85V_F$ (13, 1) but the volume for bubbles in the current experiment were between 0.67 and 0.8 of V_F. The surface tension of the water was not measured in these experiments and the addition of the fluorescent dye may have reduced it below that of pure water. Surface tension has previously been shown to reduce the bubble size at detachment due to a smaller force adhering the bubble to the orifice (8), this does not have a major effect on the dynamics of the bubble however, only changes its size and the speed of the surface tension dominated motion. Using the Minnaert Equation 3, the expected bubble resonance frequency was 1.2 kHz. This corresponds to a period of 833 µs, which will give four measurements within the initial period of the acoustic pulse when imaging at 5 kHz. The development

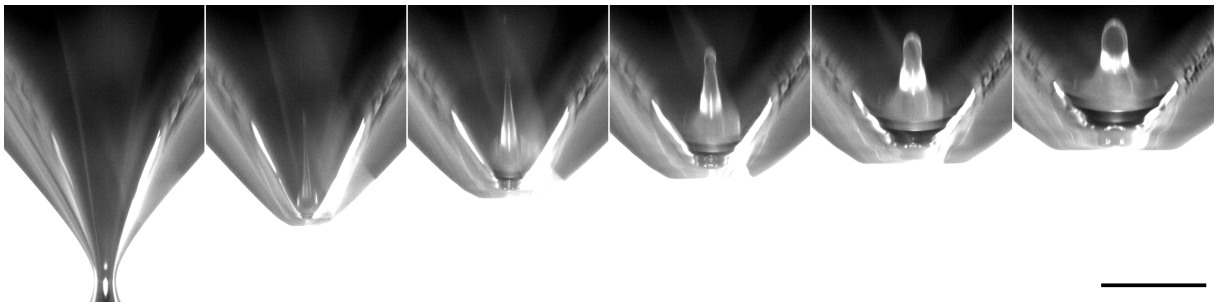

Figure 3 – Successive frames (referred to in text as A-F) of a bubble detaching with 200 µs between images. Images were captured using a combination of shadowgraphy and PLIF with a magnification of 3.8. The black line in the right-bottom corner indicates 1 mm.

and evolution of the bubble internal jet imaged using a combination of shadowgraphy and PLIF is displayed in Figure 3 with 200 µs between frames. The jet appears to grow rapidly in the first 200 µs (between frames A and B in Figure 3) following detachment although the tip is barely distinguishable, possibly due to its motion out of the plane of the laser sheet or such a small amount of light reaching the camera from the jet tip. Frames C-F of Figure 3 show the jet expanding radially with only a small increase in jet tip height. The progression of the jet tip is shown in Figure 4a, where corrections were made for the difference in size expected from viewing the jet inside the bubble. The correction was calculated by using the slope of the bubble wall in the image frame and assuming this was constant up to the apparent height of the bubble jet tip. The actual jet height was found by taking a two-dimensional profile of the bubble. A horizontal ray entering the bubble at the height that the jet appears is refracted until it reaches the axis of symmetry of the bubble and its final position is taken as the actual jet height. This correction was consistently between 2/5 and 1/3 of the jet height from

the raw images. The jet height in Figure 4a was defined as being height above the base of the bubble, which changes in each frame. This was found for five different realisations of the detachment which highlights the problem of the inherent uncertainty in time to a fixed reference point, in this case the instant of detachment. In Figure 4a the time was measured with respect to the final frame before detachment. It is clear that the jet grows very quickly in the first 400 µs after detachment and the spread of 800 µm between smallest and largest value at 200 µs indicates the first frame is very sensitive to exactly when it is taken after the detachment. This sensitivity is reduced as the growth of the jet slows so that after 1200 µs the smallest and largest jet height was within 60 µm.

At the high magnification and high speed of the images obtained from these experiments it is possible to see some asymmetries in the jet formation soon after detachment. There appears to be some bias for both the bubble detachment and initial jet development to be sloped slightly as indicated by Figure 4b, with the orange line indicating the slope in the upper region of the jet. This strong asymmetry was only apparent in the first two frames after detachment in some of the sequences recorded. The base of the bubble in the first image in Figure 4 is 33 µm wide and clearly does not have a flat profile. In the next frame, 200 µs later the upper region of the jet is tilted, but in the final frame, the tilting is not noticeable. This tendency towards axisymmetry is most likely due to the surface tension causing a pressure difference across the interface more strongly in the areas of higher curvature, quickly smoothing any asymmetric locations. The different behaviour of the jet for different bubble detachments suggests that the pinching off process is not always identical but the differences exist only for a short amount of time.

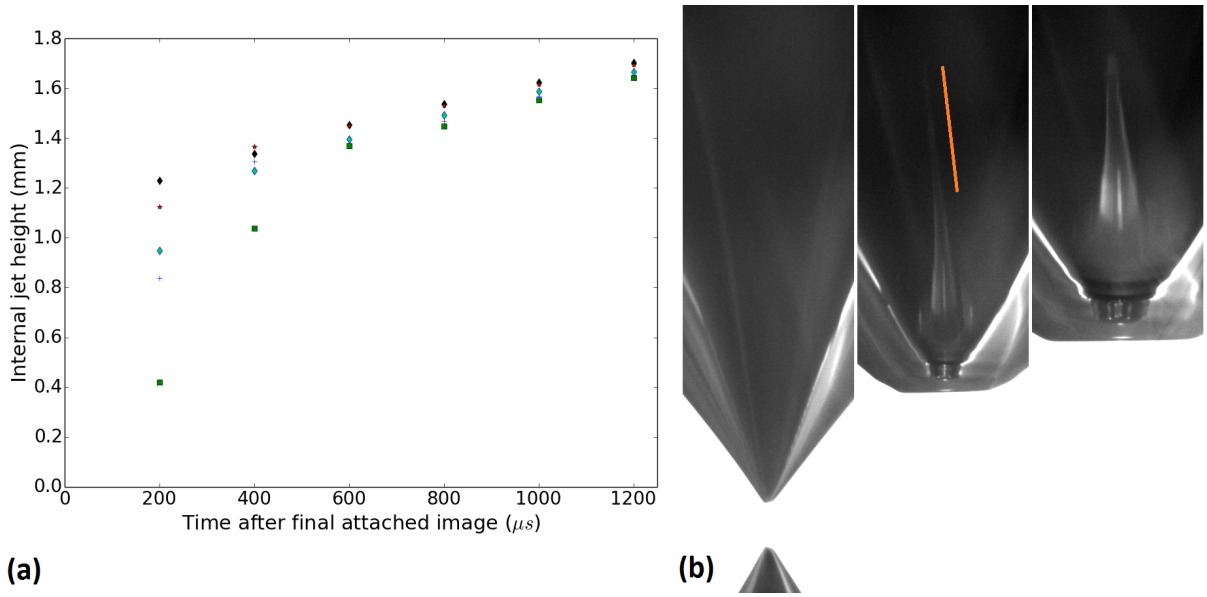

Figure 4 – (a) Height of internal jet corrected for optical effects in consecutive frames for five different bubble detachments. (b) Bubble detaching shows an asymmetric region as it detaches. This leads to a tilted internal jet (indicated in orange) which regains its symmetry in the next frame. Frames are 200 µs apart.

The tip of the internal jet grows very rapidly but within the first 400 µs after detachment there is a breakup of the jet tip occurring. This can be seen as a small faint line above the jet peak in Figure 3C, 4b (second frame) and 5 B and C. This is is barely above the noise level of the camera in these images however it is seen consistently across all bubble detachments, either in the first, second or both frames after detachment. This breakup precedes any surface waves on the bubble which appear as horizontal distortions in the PLIF and combined PLIF and shadowgraphy images but are more clear in images without backlighting by looking at the reflections of the incident laser light. These reflections are clearly seen originating from further away from the centre as the wave travels upwards on the bubble, at the same time as the horizontal distortions at these heights become apparent. This is shown in Figure 5.

4. CONCLUSIONS

Planar laser fluorescence imaging imaging of bubble detachment has allowed for some more insight into the dynamics of the bubble detachment. In this experiment the progression of the internal jet of the bubble has been measured. The internal jet can be seen rapidly growing in the first 200 µs after detachment into a thin jet which increases in width as time progresses. The high magnification of these images made it possible

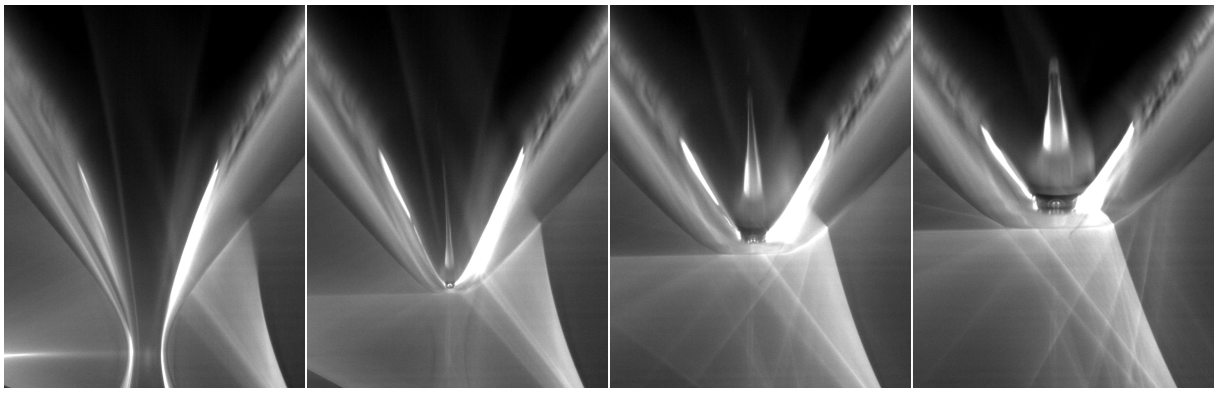

Figure 5 – Sequence of images with 200 µs between frames. shows the development of surface waves (referred to in text as A-D). In the first frame after detachment there appear to be no waves but in the final two frames new reflections off the bubble surface indicate the presence of surface waves and horizontal distortions towards the base of the bubble become clear in the final image where more surface waves have developed. Note that light is travelling from right to left.

to see sections of the jet which had broken off the top, however this phenomenon requires imaging at much higher speed and higher magnification to capture it in detail. The presence of these tip detachments was an immediate precursor to surface waves forming on the bubble moving outwards from the internal jet and their presence was seen as both horizontal distortions in the image and by light reflections at the bubble surface. As a mechanism of sound production, it is likely the forcing of the bubble by the internal jet occurs within the first 400 µs of the detachment when the growth of the internal jet is fastest. At an expected frequency of 1.2 kHz this would correspond to the first one half of a period of the acoustic emission. Given the acoustic pulse starts on a rarefaction, it appears that the initial formation of the internal jet could drive an acoustic compression in the water surrounding the bubble.

ACKNOWLEDGEMENTS

The authors acknowledge the support of the Australian Research Council through LIEF grant funding and the support of the Defence Science Technology Organisation. Marcus Fedrizzi was supported by the Australian Postgraduate Award while undertaking this research.

REFERENCES

1. Oguz HN, Prosperetti A. Dynamics of bubble growth and detachment from a needle. J Fluid Mech. 1993 12;257:111–145.

2. Thoroddsen ST, Etoh TG, Takehara K. Experiments on bubble pinch-off. Phys Fluids. 2007;19(4).

3. Longuet-Higgins MS, Kerman BR, Lunde K. Release of air bubbles from an underwater nozzle. J Fluid Mech. 1991;230:365–390.

4. Fontelos M, Snoeijer J, Eggers J. The Spatial Structure of Bubble Pinch-Off. SIAM J Appl Math. 2011;71(5):1696–1716.

5. Séon T, Antkowiak A. Large Bubble Rupture Sparks Fast Liquid Jet. Phys Rev Lett. 2012 Jul;109:014501.

6. Gekle S, Gordillo JM. Generation and breakup of Worthington jets after cavity collapse. Part 1. Jet formation. J Fluid Mech. 2010;663:293–330.

7. Deane GB, Czerski H. A mechanism stimulating sound production from air bubbles released from a nozzle. J Acoust Soc Am. 2008;123(6):EL126–EL132.

8. Czerski H, Deane GB. Contributions to the acoustic excitation of bubbles released from a nozzle. J Acoust Soc Am. 2010;128(5):2625–2634.

9. Minnaert M. XVI. On musical air-bubbles and the sounds of running water. Philosophical Magazine Series 7. 1933;16(104):235–248.

10. Buchmann N, Willert C, Soria J. Pulsed, high-power LED illumination for tomographic particle image velocimetry. Exp Fluids. 2012;53(5):1545–1560.

11. Akhmetbekov Y, Alekseenko S, Dulin V, Markovich D, Pervunin K. Planar fluorescence for round bubble imaging and its application for the study of an axisymmetric two-phase jet. Exp Fluids. 2010;48(4):615–629.

12. Nogueira S, Sousa RG, Pinto AMFR, Riethmuller ML, Campos JBLM. Simultaneous PIV and pulsed shadow technique in slug flow: a solution for optical problems. Exp Fluids. 2003;35(6):598–609.

13. Corchero G, Medina A, Higuera FJ. Effect of wetting conditions and flow rate on bubble formation at orifices submerged in water. Colloids Surf, A. 2006;290(1-3):41–49.